

UNIVERSIDAD AUTÓNOMA DEL ESTADO DE MÉXICO

Magnetic properties of FeRh clusters first principle study

by

Iasser Gutiérrez Valdés

A thesis submitted to obtain the degree of
Master in Science

at the
Departamento de Física
Facultad de Ciencias
Universidad Autónoma del Estado de México

January 2020

UNIVERSIDAD AUTÓNOMA DEL ESTADO DE MÉXICO

Abstract

Departamento de Física
Facultad de Ciencias
Universidad Autónoma del Estado de México

by Iasser Gutiérrez Valdés

“There’s plenty of room at the bottom: An Invitation to Enter a New Field of Physics” [1] was a lecture given by physicist Richard Feynman at the annual American Physical Society meeting at Caltech on December 29, 1959. Feynman considered the possibility of direct manipulation of individual atoms as a more powerful form of synthetic chemistry than those used at the time. Beginning in the 1980s, however, nanotechnology advocates cited it to establish the scientific credibility of their work.

Nanotechnology has many applications in different disciplines. For this reason, it has been studied by several groups: experimental, theoretical, and computational. These studies have proven that the size of nanoparticles can be controlled with atomic precision, which allows study specific properties like electronics and magnetism.

This thesis, the study of structure, electronic, and magnetic properties of FeRh nanoalloy will be developed, analyzing the relation between its properties with their size. The chosen topology for this study was the rhomboidal dodecahedron in two sizes Fe_8Rh_7 and $\text{Fe}_{88}\text{Rh}_{81}$.

The calculations are based on a generalized gradient approximation to density functional theory (DFT) and projected augmented wave method (PAW).

Contents

Abstract	ii
Acknowledgements	iii
List of Figures	viii
1 Introduction	1
2 Background	3
2.1 Magnetic Moment	3
2.2 Magnetization	4
2.3 Magnetic susceptibility and permeability	5
2.4 Magnetic Materials Classification	6
3 Hypothesis and Objectives	9
3.1 Hypothesis	9
3.2 General Objective	9
3.2.1 Specific Objectives	9
4 Methods	10
4.1 Schrödinger Equation	12
4.2 Adiabatic Approximation	13
4.3 Hartree-Fock Approximation	14
4.4 Bloch's Theorem	16
4.5 Hohenberg-Kohn Theorem	16
4.6 Ground State Variational Method	17
4.7 Kohn-Sham equations	18
4.8 Approximations	19
4.8.1 Local Density Approximation	19
4.8.2 Generalized Gradient Approximation	20
4.8.3 Self-Consistent Field Method	21
4.9 Projector Augmented Wave method	22
4.10 VASP	23
4.11 Computational Details	23

5	Results	24
5.1	Structural Properties	25
5.1.1	Dimers	25
5.1.2	Bulks	26
5.1.3	Nanoclusters	27
5.2	Magnetic Properties	34
5.2.1	Dimers	34
5.2.2	Bulks	35
5.2.3	Nanoclusters	37
6	Conclusions	38
	Bibliography	39

List of Figures

2.1	Paramagnetic order	6
2.2	Paramagnetic order	7
2.3	Ferromagnetic order	7
2.4	Ferrimagnetic order	8
2.5	Antiferromagnetic order	8
5.1	Ground state dimers	25
5.2	Ground state bulks	26
5.3	Fe_8Rh_7	27
5.4	First plane (Fe atoms)	28
5.5	Second plane (Rh atoms)	28
5.6	New bonds for Fe_8Rh_7	29
5.7	$\text{Fe}_{88}\text{Rh}_{81}$	29
5.8	First Fe plane	30
5.9	Second Fe plane	30
5.10	Third Fe plane	31
5.11	Distances of Fe planes	31
5.12	First Rh plane	31
5.13	Second Rh plane	32
5.14	Third Rh plane	32
5.15	Distances of Rh planes	32
5.16	New bonds for $\text{Fe}_{88}\text{Rh}_{81}$	33
5.17	DOS for dimers	34
5.18	DOS for bulks	35
5.19	DOS for nanocluster	37

List of Tables

5.1	Dimers interatomic distances	25
5.2	Bulks lattice parameters	26
5.3	Dimers magnetic moments	35
5.4	Bulks magnetic moments	36

Chapter 1

Introduction

Nanotechnology refers to an emerging and developed field of science that includes synthesis and improvement of numerous materials. Nanoparticles (NPs) are in the ranging size from 1 to 100 nm. Due to their size, these NPs may have significant differences compared with the bulk. At Present, different metallic nanomaterials are being produced and used for diverse purposes, from medical treatments, industry productions, devices of recording media storage. They also can be used in diverse materials of everyday use as cosmetics or clothes[2-5].

Nanoparticles types

Iron: They are highly reactive due to their large surface area. In the presence of oxygen and water, they rapidly oxidize to form free iron ions. They are used in medical, laboratory and industrial applications.

Rhodium: Generally are used to make Nanoalloys. Most rhodium nanoalloys are used for industrial or research purposes, such as laboratory equipment and thermocouples. Rhodium alloys are also used to coat mirrors and in search-lights, because they reflect light very well.

Nanoalloy: alloy nanoparticles show structural properties that are different from the bulk. The properties of bimetallic alloys have more advantages over ordinary metallic NPs.

Magnetic Nanoalloys: Magnetic nanoalloys are essential because of the vast range in applications, such as bioseparation, drug delivery, and biosensors. Nanotechnology has the potential to improve a wide array of tools based on nanoparticles; to become more personalized, portable, cheaper, safer, and easier to administred.

FeRh

The electronic, magnetic, and structural properties of FeRh are subject from several studies based on *density functional theory* . However, there are many ways to analyze nanoclusters, such as size, spin-polarization, alloys, chemical, and composition. At ambient conditions, the FeRh bulk is a G-type AFM, with a total magnetic moment on the Fe atoms around $3.3\mu_B$ and with a non-appreciable magnetic moment for Rh atoms. [6–10].

Chapter 2

Background

The nanoclusters have been studied exhaustively. The emphasis is mostly on nanoclusters of a single element. However, the interest in nanoalloys, particularly on binary nanoclusters, has been increasing. One of the motivations in these studies is the search for new materials for specific technological purposes. Indeed, combining elements with contrasting or complementary properties have been a better way to improve compounds and for discovering new effects and possible applicabilities. The chances to adapt the physical behavior are much more diverse in small particles than in condensed matter, due to the possibility of controlling the system size. Hence, the experimental and theoretical investigations of nanoalloys are a subject of vital importance. The study of magnetic materials is particularly challenging because it offers numerous ways of exploring competing behaviors and, their different properties compared to the molecules or bulk. One of the best candidates as a subject of study is FeRh nanoalloy for the cost and applicability.

The following section will expose some magnetic concepts and the classification of magnetic materials.

2.1 Magnetic Moment

The most direct manifestation of magnetism is the force of attraction or repulsion between magnets, which can be analogous to the Coulomb forces for electrostatically charged bodies, described by:

$$\mathbf{F} = \frac{m_1 m_2}{4\pi\mu_0 \mathbf{r}^2}, \quad (2.1)$$

where $m_1 m_2$ are the respectively body masses, separated by a distance r (m), and μ_0 is called the *permeability of vacuum* with the next value:

$$\mu_0 = 4\pi \times 10^{-7} \quad \text{henrys per meter (Hm}^{-1}\text{)} \quad (2.2)$$

It also found that an electric current exerts a force on a magnetic pole. Generally, a region of space on which a magnetic pole experiences an applied force called “*magnetic field*”. The magnetic field can be produced by other magnetic poles or by an electric current. The intensity of the field H is defined by:

$$H = ni, \quad (2.3)$$

Where i is a current flow in the winding solenoid having n turns per meter. The unit of the magnetic field is the ampere per meter Am^{-1} .

2.2 Magnetization

The differential form to express the magnetic effects are:

$$\nabla \cdot \mathbf{B} = 0, \quad \nabla \times \mathbf{B} = \mu_0 \mathbf{J} \quad (2.4)$$

This equation gets modified when the magnetic field \mathbf{B} includes a contribution from magnetized material. The divergence equation ($\nabla \cdot \mathbf{B} = 0$) came because \mathbf{B} can be written as the curl of a vector function \mathbf{A} . This result does not limit to magnetic fields produced by conventional currents.

The “curl equation” is the differential form of Ampere’s circuital law. Here it must be careful to include all types of currents that can produce a magnetic field. Hence, in the general case, this equation is correctly written as:

$$\nabla \times \mathbf{B} = \mu_0 (\mathbf{J} + \mathbf{J}_m), \quad (2.5)$$

Where \mathbf{J} is the current density, and \mathbf{J}_m is the magnetization current density, remembering the magnetization current density is the curl of the magnetization to yield:

$$\nabla \times \left(\frac{1}{\mu_0} \mathbf{B} - \mathbf{M} \right) = \mathbf{J}, \quad (2.6)$$

this is an equivalent to

$$\nabla \times \mathbf{H} = \mathbf{J} \quad (2.7)$$

where the auxiliary magnetic vector \mathbf{H} is related to the real current density through its curl.

2.3 Magnetic susceptibility and permeability

To solve problems in magnetic theory is essential to have a relationship between \mathbf{B} and \mathbf{H} or, a relationship between \mathbf{M} and one of the magnetic vectors. These relationships depend on the nature of the magnetic material. In several classes of materials, there exists an approximately linear relation between \mathbf{M} and \mathbf{H} . If the material is both isotropic or linear then,

$$\mathbf{M} = \chi_m \mathbf{H}, \quad (2.8)$$

where the dimensionless scalar quantity χ_m is called the *magnetic susceptibility*. If χ_m is positive, the material is paramagnetic, and the presence of the material strengthens the magnetic induction. If χ_m is negative, the material is called *diamagnetic*, and the presence of the material weakens the magnetic induction. Usually, χ_m is a small quantity,

$$|\chi_m| \ll 1 \text{ (for paramagnetic, diamagnetic)}. \quad (2.9)$$

A linear relationship between \mathbf{M} and \mathbf{H} implies a linear relationship between \mathbf{B} and \mathbf{H} :

$$\mathbf{B} = \mu \mathbf{H}, \quad (2.10)$$

Where the permeability μ is obtained from the combination of $\mathbf{H} = \frac{1}{\mu_0} \mathbf{B} - \mathbf{M}$, and (2.8)

$$\mu = \mu_0(1 + \chi_m). \quad (2.11)$$

2.4 Magnetic Materials Classification

A simple way to understand the susceptibility is the magnetization grade of material in the presence of an external magnetic field. All materials can be classified for the magnetic susceptibility χ as:

Diamagnetic

It means a weak magnetism, which occurs in a material containing no atomic magnetic moments. The relative susceptibility of such a material is negative and small, typically $\bar{\chi} \simeq 10^{-5}$.

Diamagnetism is a property of all materials, and always makes a weak contribution to the material's response to a magnetic field. However, other forms of magnetism are so much stronger than when multiple different types of magnetism are present in a material; the diamagnetic contribution is usually negligible.

Diamagnetism

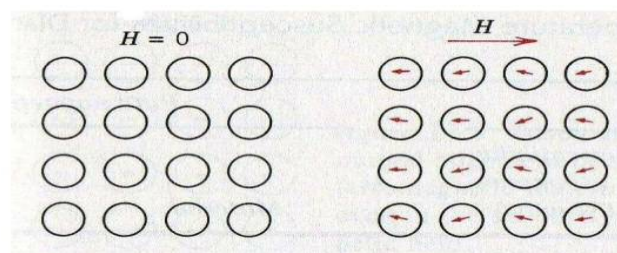


FIGURE 2.1: They are repelled by the applied magnetic field.

Paramagnetic

It refers to a feeble magnetism, which has positive susceptibility of the order of $\bar{\chi} = 10^{-3} - 10^{-5}$, this magnetic behavior is found in materials that contain magnetic atoms or ions with a considerable separated distance between each other. They have no appreciable interaction with one another.

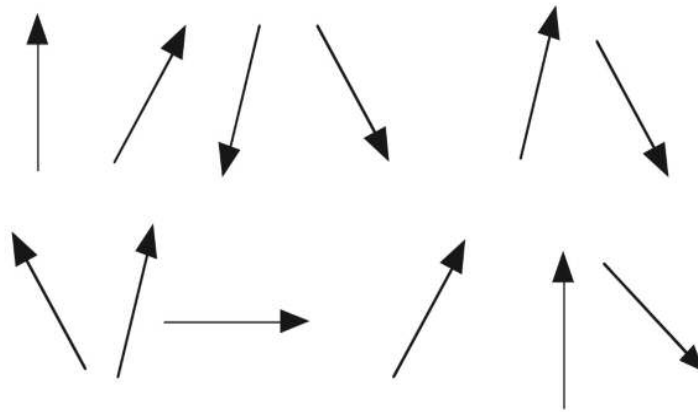


FIGURE 2.2: Spins are randomly oriented in presence of an external magnetic field.

Ferromagnetic

This term is used to denote strongly magnetic behavior, like the strong attraction of a material to a permanent magnet. The origin of this strong magnetism is the presence of a spontaneous magnetization produced by parallel alignment of spins. Instead of parallel arrangement of all spins, there can be an anti-parallel alignment of unequal spins.

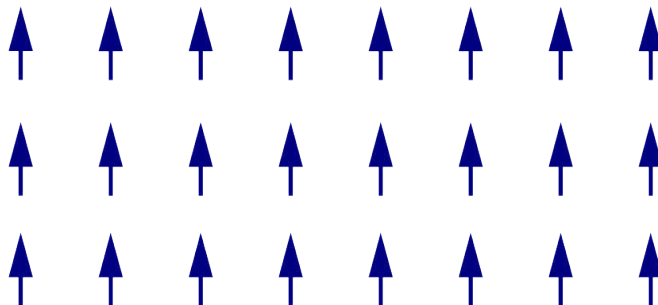


FIGURE 2.3: Spins are aligned parallel in magnetic domains.

Ferrimagnetic

For ferrimagnets, the A and B-sublattices are occupied by different magnetic atoms and sometimes by different numbers of particles. The antiferromagnet spin arrangement results in an uncompensated spontaneous magnetization.

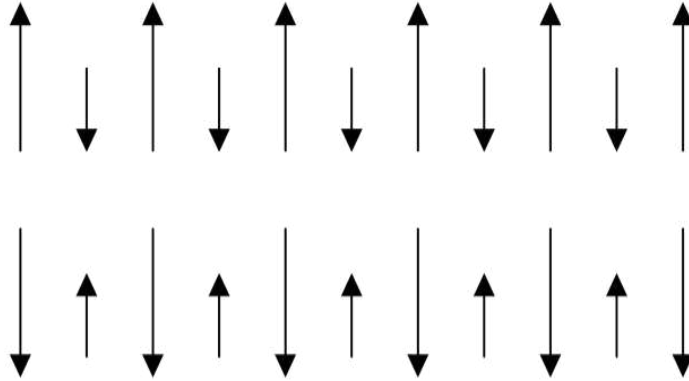


FIGURE 2.4: Spins are aligned antiparallel but do not cancel.

Antiferromagnetic

For antiferromagnetic materials, the closest spins align antiparallel to one another, and their magnetic moments cancel. Therefore, an antiferromagnet produces no spontaneous magnetization and shows a weak magnetism. The relative magnetic susceptibility for antiferromagnetic materials ranges from 10^{-2} to 10^{-5} almost the same as paramagnets. The only difference lies in the presence of an ordered spin structure. When an external magnetic field is applied parallel to the spin axis, the spins which are parallel and antiparallel to the field have almost no torque, in other words, they keep their ordered spin arrangement, this is the reason why the susceptibility, in this case, is smaller than for a normal paramagnet [11–15].

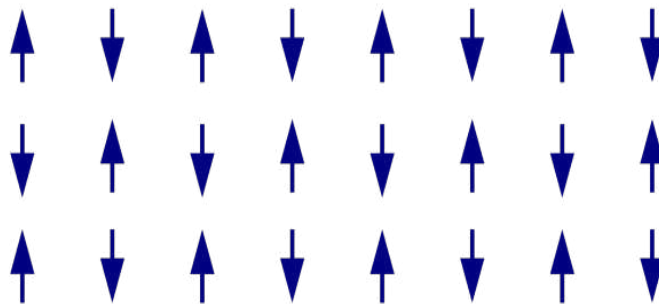


FIGURE 2.5: Spins are aligned antiparallel in magnetic domains.

Chapter 3

Hypothesis and Objectives

3.1 Hypothesis

To change the nanocluster size will modify the electronic and magnetic properties.

3.2 General Objective

To simulate the physical properties for two FeRh nanoclusters (Fe_8Rh_7 and $\text{Fe}_{88}\text{Rh}_{81}$) in the framework of first principles molecular dynamic, taking into account the spin polarization.

3.2.1 Specific Objectives

- 1.- To find a relation between the size and magnetic moment for each nanocluster.
- 2.- To study electronic and magnetic properties using the density of states of the respective nanocluster.
- 3.- To compare the results with previous experimental and theoretical studies.

Chapter 4

Methods

This section will present a detailed summary of the approximations that built DFT; this way, the reader could have a proper perspective about this theory and its scope in the nanoparticles study.

An ab initio method aims to find the solution to the many-body Schrödinger equation section 4.1, which plays the role of Newton's laws and conservation energy in classical dynamics, its purpose is to predict the future behavior of a dynamic system. The first simplification to this goal is the Born Oppenheimer approximation (Adiabatic approximation) section 4.2, whereby the electronic and nuclear degrees of freedom are separated, this division is due to the electrons are much less massive than the nuclei but experience similar forces, consequently, the electrons will respond instantaneously to the movement of the nuclei.

Another approximation to take into account is the Hartree-Fock approximation. In quantum mechanics many problems are about atoms, molecules and involve several electrons around some atomic nuclei. The Hartree-Fock approximation is one of the most important ways to solve this kind of problem, the key to this method, are the assumptions it makes about the electron wave function described in section 4.3.

Section 4.4 contains Bloch's theorem, which is a wave composed of a plane wave modulated by a periodic function and allows the study of crystalline systems.

In 1964 Pierre Hohenberg and Walter Kohn demonstrated that there is a one to one relationship between electronic density and external potential in the fundamental state, which equations will be exposed section 4.5.

The variational method section 4.6, is another main approximation used in quantum mechanics, the basic idea is to guess a “trial” wavefunction for the problem, which consists of some adjustable parameters called “variational parameters”. These parameters are adjusted until the energy of the trial wavefunction is minimized.

Considering all the previous methods and approaches it is no longer the Schrödinger equation solution need to find the energy of the system but, the Kohn-Sham equations section 4.7, which instead of electron pair interactions, considers an electronic charge density that will be equal to that of the fundamental state and all the physical properties of the system will functionally depend on it. Section 4.8 contains the main approximation that helps Kohn-Sham equations.

The projector augmented wave method (PAW) section 4.9 is a technique used in ab initio calculations. It is a generalization of the pseudopotential and linear augmented-plane-wave methods and allows DFT calculations to have higher computational efficiency. The main idea of PAW is to divide the system into two regions, one for the core where it uses a projection of the spherical harmonics and a second region where all the valence electrons are found, it uses plane waves.

All this theory is implemented in the software VASP, which the applications are described in section 4.10.

Section 4.11 contains all the computational details that were used in the simulation of the nanoclusters.

4.1 Schrödinger Equation

The equation to find the total energy of a many particles (electrons and ions) system is the Schrödinger equation.

The Schrödinger equation time exclude is used for any electronic structure of matter but, for most cases, it is only for problems with atoms and molecules without time-depended interactions. In the case of $n - electron$ isolated in an atomic or molecular system, the Schrödinger equation is:

$$\hat{H}\Psi = E\Psi, \quad (4.1)$$

where E is the electronic energy, $\Psi = \Psi(x_0, x_1, x_2, x_3, \dots, x_n)$ is the wave function, and \hat{H} is the Hamiltonian operator.

With some special considerations explained in section 4.2, the Schrödinger equation can be described in atomic coordinates as:

$$\hat{H} = \sum_{i=1}^N \left(-\frac{1}{2} \right) \nabla_i^2 + \sum_{i=1}^N v(\mathbf{r}_i) + \sum_{i<j}^N \frac{1}{r_{ij}}, \quad (4.2)$$

for which,

$$v(\mathbf{r}_i) = \sum_{\alpha} \frac{Z_{\alpha}}{r_{i\alpha}}, \quad (4.3)$$

this is the external potential which acts in the i -th electron, the potential due to the core charge Z_{α} , r_i and r_j are the distances of the $i - th$ and the $j - th$ electrons, and r_{ij} is the difference between them.

The equation (4.2) can be rewritten as:

$$\hat{H} = \hat{T} + \hat{V}_{ee} + \hat{V}_{ne}, \quad (4.4)$$

where

$$\hat{T} = \sum_{i=1}^N \left(-\frac{1}{2} \nabla_i^2 \right), \quad (4.5)$$

is the operator's Kinect energy, the second part is the operator's repulsion electron-electron energy described as:

$$\hat{V}_{ee} = \sum_{i < j}^N \frac{1}{r_{ij}}, \quad (4.6)$$

and the last term is the electron-core interaction, (being M the number of ions) described by:

$$V_{ne} = \sum_i^N \sum_{\alpha}^M \frac{Z_{\alpha}}{r_{i\alpha}}, \quad (4.7)$$

the total energy W is the electronic energy E , plus the repulsion energy due to the core-core interaction.

$$V_{nn} = \sum_{\alpha < \beta} \frac{Z_{\alpha} Z_{\beta}}{R_{\alpha\beta}}, \quad (4.8)$$

this is

$$W = E + V_{nn}. \quad (4.9)$$

Is indifferent to solve 4.4 because includes E and V_{nn} in the Hamiltonian's definition \hat{H} , and it works to solve Schrödinger's equation in the form $\hat{H}\Psi = W\Psi$. This equation is solved with the appropriate boundary conditions, particulrally, when Ψ decays from zero to infinite due an atom or molecule; and $|\Psi|^2$ is a distribution probability, such as,

$$|\Psi(r^N, s^N)|^2 dr^N, \quad (4.10)$$

where s are the spin coordinates[16–18].

4.2 Adiabatic Approximation

The Schrödinger equation for many particles can be written as:

$$\left[\begin{aligned} & -\hbar^2 \left(\sum_i \frac{\hbar_i^2}{2m_e} + \sum_j \frac{\hbar_j^2}{2M_n} \right) + \sum_i \sum_{i \neq l} \frac{e^2}{4\pi\epsilon_0 |r_i - r_l|} \\ & + \sum_i \sum_{i \neq k} \frac{Z_j Z_k e^2}{4\pi\epsilon_0 |R_i - R_k|} - \sum_i \sum_{i \neq k} \frac{Z_k e^2}{4\pi\epsilon_0 |r_i - R_k|} \end{aligned} \right] \Psi = E\Psi. \quad (4.11)$$

However, specific considerations must be taken into account to simplify it.

Considering the ion's mass is much bigger than electron's; therefore, the kinetic energy of ions may be omitted,

$$M_n \gg m_e.$$

The ion-ion interaction is constant because the ions are fixed, hence only the electron-electron and electron-ion interactions are considered:

$$\sum_i \sum_{i \neq k} \frac{Z_j Z_k e^2}{4\pi\epsilon_0 |R_i - R_k|},$$

thus the Schödinger's equation can be rewritten as [19, 20]:

$$\frac{1}{2} \left[-\hbar^2 \left(\sum_i \frac{\nabla_i^2}{2m_e} \right) + \sum_i \sum_{i \neq l} \frac{e^2}{4\pi\epsilon_0 |r_i - r_l|} - \sum_i \sum_{i \neq k} \frac{Z_k e^2}{4\pi\epsilon_0 |r_i - R_k|} \right] \Psi_e = E\Psi_e. \quad (4.12)$$

4.3 Hartree-Fock Approximation

Using N-order Slater's determinant is the way to find the wave function for an N-electron system, this wave function for all electrons is antisymmetric, obeys Pauli's exclusion principle, and it is described as:

$$\begin{aligned} \Psi_{HF} &= \frac{1}{\sqrt{N!}} \begin{bmatrix} \psi_1(x_1) & \psi_2(x_1) & \dots & \psi_N(x_1) \\ \psi_1(x_2) & \psi_2(x_2) & \dots & \psi_N(x_2) \\ \vdots & \vdots & \ddots & \vdots \\ \psi_1(x_N) & \psi_2(x_N) & \dots & \psi_N(x_N) \end{bmatrix} \\ &= \frac{1}{\sqrt{N!}} \det[\psi_1 \psi_2 \dots \psi_N]. \end{aligned} \quad (4.13)$$

The simplest case of Slater's determinant (for two electrons) it will be used to prove the antisymmetry property of the wave function,

$$\begin{aligned}\Psi &= \frac{1}{\sqrt{2!}} \begin{bmatrix} \psi_1(x_1) & \psi_2(x_1) \\ \psi_1(x_2) & \psi_2(x_2) \end{bmatrix} \\ &= \frac{1}{\sqrt{2!}} [\psi_1(x_1)\psi_2(x_2) - \psi_1(x_2)\psi_2(x_1)]\end{aligned}\quad (4.14)$$

since, it treats it with indistinguishable electrons, it can express the determinant in a generalized form as:

$$\begin{aligned}\Psi &= \frac{1}{\sqrt{2!}} \begin{bmatrix} \sum_i^N \psi_i(x_1) & \sum_j^N \psi_j(x_1) \\ \sum_i^N \psi_i(x_2) & \sum_j^N \psi_j(x_2) \end{bmatrix} \\ &= \frac{1}{\sqrt{2!}} \left[\sum_i^N \psi_i(x_1) \sum_j^N \psi_j(x_2) - \sum_i^N \psi_i(x_2) \sum_j^N \psi_j(x_1) \right],\end{aligned}\quad (4.15)$$

by notation $\sum_i^N \psi_i = \psi_i(x_1)$.

The Hartree-Fock approximation is the method by which the orthonormal orbitals ψ_i simplifies the determinant form Ψ ; the normalization of the integral $\langle \Psi_{HF} | \Psi_{HF} \rangle$ is equal to 1, and the following equation finds the value of the expectation energy:

$$E_{HF} = \langle \Psi_{HF} | \hat{H} | \Psi_{HF} \rangle = \sum_{i=1}^N H_i + \frac{1}{2} \sum_{i,j}^N (J_{ij} - K_{ij}), \quad (4.16)$$

where,

$$H_i = \int \psi_i^*(x) \left[-\frac{1}{2} \nabla^2 + v(\mathbf{r}) \right] \psi_i(x) dx, \quad (4.17)$$

$$J_{ij} = \int \int \psi_i(x_1) \psi_i^*(x_1) \frac{1}{r_{12}} \psi_j^*(x_2) \psi_j(x_2) dx_1 dx_2, \quad (4.18)$$

$$K_{ij} = \int \int \psi_i(x_1) \psi_j^*(x_1) \frac{1}{r_{12}} \psi_i^*(x_2) \psi_j(x_2) dx_1 dx_2, \quad (4.19)$$

these integrals are real and with the condition $J_{ij} \leq K_{ij} \leq 0$. The term J_{ij} are the coulombians integrals, and K_{ij} are the exchange integrals. These terms have important equality:

$$J_{ii} = K_{ii} \quad (4.20)$$

thus the double integral (4.16) can have the terms $i = j$ [17, 19, 20].

4.4 Bloch's Theorem

For a crystalline solid, the ionic potential with any translation \mathbf{R} , is described in unitvectors terms as:

$$v(\mathbf{r}) = v(\mathbf{r} + \mathbf{R}), \quad (4.21)$$

and the wave function as:

$$\psi(\mathbf{r}) = \psi(\mathbf{r} + \mathbf{R}) \quad (4.22)$$

The Bloch's theorems say, in a solid periodic system, each electronic wave function is the product of a periodical lattice and a wave part.

$$\psi_i(\mathbf{r}) = u_i e^{i\mathbf{k}\cdot\mathbf{r}}, \quad (4.23)$$

where the function u_i has the same periodicity as the lattice, ergo $u_i(x) = u_i(x + a)$, being a the lattice period. It means the auto functions of the wave equation for a periodic crystalline potential, are the product of a plane wave and another periodic function with a period of the crystalline lattice. An important factor is the nature of the wavenumber $k = \frac{(2\pi)}{\lambda}$, which the electron's energy E depends on. The energetic relations is known as "dispersion relation" and can obtain a significant quantity on information about the electronic properties from a crystal, such as the density of states or the carriers effective mass [21].

4.5 Hohenberg-Kohn Theorem

The Hohenberg-Kohn approximation is used to formulate the Density Functional Theory as an exact theory for many particles system, applicable to systems with particles interactions,

$$\begin{array}{ccc}
V_{ext}(\mathbf{r}) & \longleftarrow & n_0(\mathbf{r}) \\
\Downarrow & & \Uparrow \\
\Psi_i(\{\mathbf{r}\}) & \Rightarrow & \Psi_0(\{\mathbf{r}\})
\end{array}$$

This is a scheme of the Hohenberg-Kohn theorem, where the small arrows represent a solution of the Schrödinger equation, where the potential V_{ext} determines all the states by itself $\Psi_i(\{\mathbf{r}\})$, including the ground state $\Psi_0(\{\mathbf{r}\})$ and the density of the ground state $n_0(\mathbf{r})$. The long arrow represents the Hohenberg-Kohn, which complete the cycle.

Theorem I: For each particle system interacting in an external potential $V_{ext}(\mathbf{r})$, the potential $V_{ext}(\mathbf{r})$ is singularly chosen, except for the density of the ground state $n_0(\mathbf{r})$.

Corollary I: Since the Hamiltonian is entirely determined, except for a constant energy change, can be deduced the wave functions of several states (ground and excited). Thus, the system properties are determined and only give the density of the ground state $n_0(\mathbf{r})$.

Theorem II: An universal functional for the energy $E[n]$ can be defined in terms of the density $n(\mathbf{r})$, valid for any external potential $V_{ext}(\mathbf{r})$. The energy of the ground state is exactly to the value of the global minimum functional and to the density $n(\mathbf{r})$ that minimize the ground state density $n_0 functional(\mathbf{r})$.

Corollary II: The functional $E[n]$ only works to determine the energy and the exact density of the ground state. In general, the excited states of the electrons have to be determined by other ways and the thermal equilibrium properties such as the specific heat are determined directly for the free energy density functional [21, 22].

4.6 Ground State Variational Method

For ground state energy calculation, it is necessary to minimize the value of the total energy E . When a system is in the state Ψ , can or can not satisfy (4.1). The average energies measurement is given by:

$$E[\Psi] = \frac{\langle \Psi | \hat{H} | \Psi \rangle}{\langle \Psi | \Psi \rangle}, \quad (4.24)$$

where

$$\langle \Psi | \hat{H} | \Psi \rangle = \int \Psi^* \hat{H} \Psi dx, \quad (4.25)$$

is the energy for each measure given by the values of \hat{H} . Hence; the energy will be equal or bigger than the ground state energy but, never smaller

$$E[\Psi] \geq E_0. \quad (4.26)$$

The energy can be calculated by a Ψ whose is above the true ground state energy E . The full minimization of the functional $E[\Psi]$ is for all the allowed wave functions, in an N electrons systems; they will give the ground state Ψ_0 and the energy $E[\Psi_0] = E_0$. This is the formal proof of “minimum energy principle”; and expanding Ψ in terms of the normalized eigenstates of \hat{H} , Ψ_k :

$$\Psi = \sum_k C_k \Psi_k, \quad (4.27)$$

the energy becomes

$$E[\Psi] = \frac{\sum_k |C_k|^2 E_k}{\sum_k |C_k|^2} \quad (4.28)$$

Where E_k is the K eigenstate’s energy of \hat{H} . Including the Ψ_k orthogonality. Because $E_0 \leq E_1 \leq E_2 \dots$ $E[\Psi]$ is always bigger or equal to E_0 , and it finds the minimum if and only if $\Psi = C_0 \Psi_0$. Each eigenstate Ψ is a boundary of the functional $E[\Psi]$, this means, it can replace the Schödinger’s equation $\hat{H}\Psi = E\Psi$ with the variational principle [23].

$$\delta E[\Psi] = 0 \quad (4.29)$$

4.7 Kohn-Sham equations

Kohn and Sham presented a way to approximate the universal functional, to achieve it they developed a “fictional system” which is constituted by a system of not interacting electrons, where the energy contributions of the system are described by:

$$\begin{aligned} E[\rho_i] = & 2 \sum_i \int \psi_i \left[\frac{-\hbar^2}{2m} \right] \nabla^2 \psi_i dr^3 + \int V_n(\mathbf{r}) n(\mathbf{r}) dr^3 \\ & + \frac{e^2}{2} \int \frac{n(\mathbf{r}) n(\mathbf{r}')}{|\mathbf{r} - \mathbf{r}'|} dr^3 dr'^3 + E_{XC}[n(\mathbf{r})] + E_n(R_i) \end{aligned} \quad (4.30)$$

Where E_n is the coulomb energy associated with the interactions between cores in the R_i positions, V_n is the total static potential electron-ion, $E_{XC}[n(\mathbf{r})]$ is the exchange-correlation functional, and $n(\mathbf{r})$ is the electronic charge density given by:

$$n(\mathbf{r}) = 2 \sum_i |\psi_i(\mathbf{r})|^2, \quad (4.31)$$

only the minimum value of Kohn-Sham equations has physics meaning, and is equal to the minimum energy value of the system formed by electrons and ions in the R_i positions. The wave function ψ_i minimize the Kohn-Sham energy functional, given by the self-consistent solutions,

$$\left[\frac{-\hbar^2}{2m} \nabla^2 + V_n[\rho] + V_H[\rho] + V_{XC}[\rho] \right] \psi_i(\mathbf{r}) = \epsilon_i \psi_i(\mathbf{r}), \quad (4.32)$$

where ψ_i is the wave function of the electronic state i , ϵ_i is the the eigenvalue of Kohn-Sham, and V_H is the Hartree potential of the electrons given by:

$$V_H = e^2 \int \frac{n(r)}{|r - r|} dr^3, \quad (4.33)$$

the exchange-correlation potential, V_{XC} , is described by:

$$V_{XC}(\mathbf{r}) = \frac{\delta E_{XC}[n(\mathbf{r})]}{\delta n(\mathbf{r})}. \quad (4.34)$$

The Kohn-Sham equations represent a mapping from a system formed by many particles to a system with only an effective potential due to all the electrons [23].

4.8 Approximations

4.8.1 Local Density Approximation

Is an analogy to the Schrödinger for an interacting N-electrons system. To ease the energy calculations, The system has to be treated like a single electron system without interaction and immersed in an effective potential. However, Does not exist a functional way to find exchange-correlation energy; the Kohn-Sham equations do not provide a form for this energy, this is necessary to make use of approximation along to DFT to find this energy. A useful approximation is the “Local Density Approximation, (LDA)”, where the exchange-correlation energy in \mathbf{r} depends on the density at the same point,

$$E_{XC}[\rho] = \int \epsilon_{XC}[\rho]\rho(\mathbf{r})d^3r, \quad (4.35)$$

where $\epsilon_{XC}[\rho]$ is the exchange-correlation energy from an electron in an electronic gas without interactions and with a uniform density. Each point $|\mathbf{r}|$ has associated a charge density, and every point in the system has an exchange-correlation energy. The changes in the density are very small.

The correspondence for the effective potential and the exchange-correlation potential are described by:

$$v_{eff} = v(\mathbf{r}) + \int \frac{\rho(\mathbf{r}')d\mathbf{r}'}{|\mathbf{r} - \mathbf{r}'|} + \frac{\delta E_{XC}[\rho]}{\delta \rho(\mathbf{r})} = v(\mathbf{r}) + \int \frac{\rho(\mathbf{r}')d\mathbf{r}'}{|\mathbf{r} - \mathbf{r}'|} + V_{XC}^{LDA}, \quad (4.36)$$

according to the equation 4.35 the exchange-correlation potential term for LDA is:

$$V_{XC}^{LDA} = \frac{\delta}{\delta \rho(\mathbf{r})} \int (\epsilon_{XC}[\rho]\rho(\mathbf{r})d^3r) = \epsilon_{XC}(\rho(\mathbf{r})) + \rho(\mathbf{r}) \frac{\delta \epsilon_{XC}(\rho(\mathbf{r}))}{\delta \rho(\mathbf{r})} \quad (4.37)$$

and ϵ_{XC} can be separate in two terms :

$$\epsilon_{XC} = \epsilon_x + \epsilon_c, \quad (4.38)$$

one term is for exchange and the other for correlation; thus, can simplify the problem, and using the Dirac's functional can be found:

$$\epsilon_x(\rho) = -C_x \rho^{\frac{1}{3}}(\mathbf{r}) \quad C_x = \frac{3}{4} \left(\frac{3}{\pi} \right)^{\frac{1}{3}}, \quad (4.39)$$

leaving the appropriate numerical calculations for the ϵ_c term [17, 24, 25].

4.8.2 Generalized Gradient Approximation

For the approximation of the generalized gradient (GGA), the term exchange-correlation depends on the density of spin.

$$\rho_{\uparrow}(\mathbf{r}) \quad \text{and} \quad \rho_{\downarrow}(\mathbf{r}) \quad (4.40)$$

where, for a small densities variance, the local spin density approximation (LSDA) is written by:

$$E_{XC}^{LSDA} = \int d^3\mathbf{r} \rho(\mathbf{r}) \epsilon_{XC}(\rho_{\uparrow}, \rho_{\downarrow}), \quad (4.41)$$

where $\rho(\mathbf{r})$ is the total density defines as follow $\rho(\mathbf{r}) = (\rho_{\uparrow} + \rho_{\downarrow})$; however, the GGA approximation is more general because it takes into account changes in the topological form of density:

$$\nabla\rho_{\uparrow}(\mathbf{r}) \quad \text{and} \quad \nabla\rho_{\downarrow}(\mathbf{r}) \quad (4.42)$$

considering 4.41 the exchange-correlation term can be written as:

$$E_{XC}^{GGA} = \int d^3\mathbf{r} \rho(\mathbf{r}) \epsilon_{XC}(\rho_{\uparrow}, \rho_{\downarrow}; \nabla\rho_{\uparrow}, \nabla\rho_{\downarrow}), \quad (4.43)$$

for the term of the exchange-correlation potential, the variation of the functional it can express as:

$$\delta E_{XC}^{GGA} = \int d^3\mathbf{r} \left[\epsilon_{XC} + \rho \frac{\delta\epsilon_{XC}}{\delta\rho_{\uparrow\downarrow}} + \rho \frac{\delta\epsilon_{XC}}{\delta\nabla\rho_{\uparrow\downarrow}} \right] \delta\rho(\mathbf{r}), \quad (4.44)$$

thus, the exchange-correlation potential has the form:

$$V_{XC}^{GGA} = \int d^3\mathbf{r} \left[\epsilon_{XC} + \rho \frac{\delta\epsilon_{XC}}{\delta\rho_{\uparrow\downarrow}} + \rho \frac{\delta\epsilon_{XC}}{\delta\nabla\rho_{\uparrow\downarrow}} \right], \quad (4.45)$$

this equation is more general than (4.41) and considers variation terms from the gradient. Hence, it can get more detailed results for better visualization of the charge pseudo-density [24, 25].

4.8.3 Self-Consistent Field Method

In the DFT, the fundamental quantity calculated by the self-consistent field method (SCF) is the charge density. The calculations are made in cycles and stops when converging until the ground state density.

For this method, the pseudo-potential interaction for each ion has to be obtained. First, propose a wave function to give shape to the charge density to calculate the exchange-correlation potential. The Kohn-Sham equations must be diagonalized to obtain the

eigenstates. Then, has to calculate a new density and, if it is self-consistent with the first proposed is the total energy charge density; otherwise, another charge density has to be generated [23, 25].

4.9 Projector Augmented Wave method

The AE (all-electron) wave functions Ψ_{nk} , with an n index, corresponds to a summation over the bands and k indexing the k-points, they obtain starting from PS (pseudo) ones Ψ'_{nk} by using a linear transformation:

$$|\Psi_{nk}\rangle = |\Psi'_{nk}\rangle + \sum_i (|\Phi_i\rangle - |\Phi'_i\rangle) \langle p_i | \Psi'_{nk} \rangle, \quad (4.46)$$

where the index i stands for the atomic position \vec{R} , the angular momentum (l, m) and index n to label different partial waves for the same site and angular momentum. The AE Φ_i and PS Φ'_i partial waves are equal outside the PAW sphere. Hence, $\Psi_n = \Psi'_n$ outside a core radius r_c^l . The projectors p'_i are dual to the PS partial waves:

$$\langle p'_i | \Phi'_j \rangle = \delta_{ij}. \quad (4.47)$$

PAW method, use two grids: a radial inside the PAW sphere and a regular mesh in the whole simulation cell, ergo, the partial waves and projector functions set apart in angular and radial parts:

$$\begin{aligned} \Phi_i(\vec{r}) &= \frac{\Phi_{n_i l_i}(\mathbf{r})}{\mathbf{r}} S_{l_i m_i}(\hat{\mathbf{r}}); \Phi'_i(\vec{r}) = \frac{\Phi'_{n_i l_i}(\mathbf{r})}{\mathbf{r}} S_{l_i m_i}(\hat{\mathbf{r}}), \\ p'_i(\vec{r}) &= \frac{p'_{n_i l_i}(\mathbf{r})}{\mathbf{r}} S_{l_i m_i}(\hat{\mathbf{r}}) \end{aligned}, \quad (4.48)$$

with $S_{lm}(\hat{\mathbf{r}})$ the real spherical harmonics. On the other hand, the pseudized wave functions are expanded on a plane wave basis set:

$$\Psi'_{nk}(\vec{r}) = \sqrt{\frac{1}{\Omega}} \sum_{\vec{G}} c_{nk}(\vec{G}) e^{i(\vec{K} + \vec{G}) \cdot \vec{r}}, \quad (4.49)$$

with Ω the volume of the unit cell [26].

4.10 VASP

“The Vienna Ab initio Simulation Package (VASP) is a computer program for atomic scale materials modelling, e.g. electronic structure calculations and quantum-mechanical molecular dynamics, from first principles.

VASP computes an approximate solution to the many-body Schrödinger equation, either within density functional theory (DFT), solving the Kohn-Sham equations, or within the Hartree-Fock (HF) approximation, solving the Roothaan equations. Hybrid functionals that mix the Hartree-Fock approach with density functional theory are implemented as well” [27].

4.11 Computational Details

This work is based on the density functional theory (DFT), implemented in The Vienna ab initio simulations package (VASP). In this software, the exchange and correlation energy are described using the spin-polarized local density approximation (LDA) and Perdew and Wang’s generalized gradient approximation (GGA). VASP solves the Kohn-Sham equations considering the spin polarization, and taking into account the core electrons with the projector augmented wave (PAW) method, which is an all-electron frozen-core approach that allows include the nodes of valence KS orbitals in the core region and the effects on the electronic structure, total energy, and interatomic forces [17, 24, 26, 28]. The wave functions were expanded in a plane wave basis set with an energy cutoff $E_{max} = 248$ eV. A simple cubic supercell worked as the periodic boundary condition, where the side sizes were 30.0 Å for the dimer and bulk study, 35.0 Å for the smallest nanocluster and 49.0 Å for the larger. The discrete energy levels are broadened using Gaussian smearing $\sigma = 0.02$ eV to speed up the system convergence. Since the interested is limited systems, The chosen K-points for dimers and bulk were 10 10 10, and for nanoclusters the Γ point restricted the reciprocal space summations [29–33]. The structures analyzed were the dimers and bulks of Fe, Rh, and Fe-Rh nanoclusters with a *rhomboidal dodecahedron* topology, varying number of atoms in the edge, resulting in nanoclusters of Fe_8Rh_7 and $Fe_{88}Rh_{81}$ with an initial interatomic distance of 2.98 Å [34–37].

Chapter 5

Results

Section 5.1 presents the structural properties obtained in this work, dividing into three subsections, 5.1.1 contains the analysis of the interatomic distance for Fe₂, Rh₂, and FeRh dimers. Table 5.1 shows the values for dimers obtained from this work and the literature. 5.1.2 consists of the analysis of the lattice parameter for Fe, Rh, and FeRh bulks. Table 5.2 shows the values obtained from this work and the literature. 5.2.3 contains all the interatomic distances (figure 1 and figure 2) for the FeRh nanoclusters after the relaxation process.

Section 5.3 comprehend three subsections, 5.3.1 shows the density of states (DOS) for Fe, Rh, and FeRh dimers and the value for the total magnetic moment obtained, 5.3.2 exposes the DOS for Fe, Rh, and FeRh bulks including the magnetic moment (total and per atom), 5.3.3 contains the DOS comparison of FeRh nanoclusters and bulks with their respective magnetic moment value.

All the results for FeRh (magnetic moment and interatomic distances) from this work and literature are in Table 5.3.

5.1 Structural Properties

5.1.1 Dimers

The dimers allow inferring useful trends about the different types of bonds found in bulks and nanoclusters. The following subsection presents the results for Fe_2 , Rh_2 , and FeRh dimers.

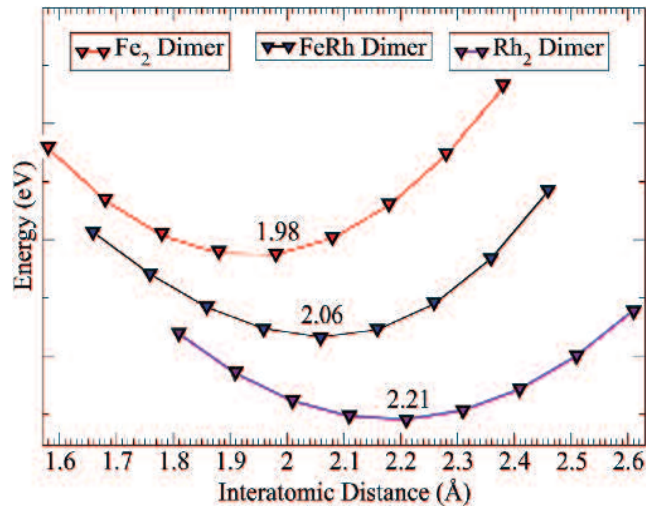


FIGURE 5.1: This figure shows the ground-state interatomic distance value for Fe_2 (red), Rh_2 (violet), and FeRh dimers (black).

The numerical value presented corresponds to the minimum energy bonding distance. The Rh_2 dimer has the largest interatomic distance followed by FeRh and Fe_2 being the smallest, the increase in the bond length is due to the size of the atomic radii for each element, this is present in how the values tend to shift to the right in the interatomic distance axis. The results are comparing with previous theoretical and experimental studies in Table 5.1.

Interatomic distance (Å)			
Dimer	Fe_2	FeRh	Rh_2
This Work	1.98	2.06	2.21
Theoretical			
Ref. [38]	1.98	2.07	2.21
Experiment			
Ref. [39]	2.02		
Ref. [40]		1.80	
Ref. [41]			2.12

TABLE 5.1: Interatomic distances results found for Fe_2 , Rh_2 , and FeRh dimers compared with theoretical and experimental results.

The results of this work match the theoretical results except for a slight difference of 0.01 Å in the FeRh bond contrary to the experimental results that have a significant difference compared with these results, being the Rh dimer the largest difference, follow by FeRh and Fe₂ having the closest value.

5.1.2 Bulks

The study of the bulks is essential to understand the behavior and changes of nanocluster's properties. This subsection contains the results for Fe, Rh, and FeRh bulks. The Figure 5.2 shows the lattice parameter value of each bulk and Table 5.2 presents the comparison of the results of this work with previous studies.

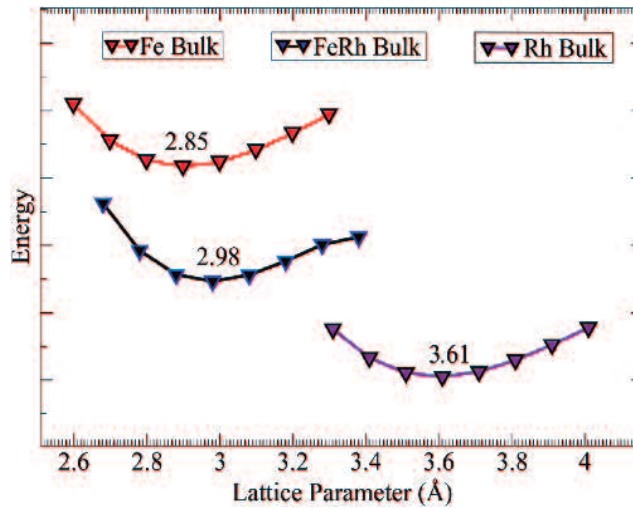


FIGURE 5.2: This figure shows the comparison of the ground-state lattice parameter of Fe (red), Rh (violet), and FeRh (black) Bulks.

Lattice Parameter (Å)			
Bulk	Fe	FeRh	Rh
This Work	2.85	2.98	3.61
Theoretical			
Ref. [42]	2.85		
Ref. [43]		3.01	
Ref. [44]			3.76
Experiment			
Ref. [45]	2.86		
Ref. [46]		2.98	
Ref. [47]			3.84

TABLE 5.2: Lattice parameter results found for Fe, Rh, and FeRh bulks compared with theoretical and experimental results.

The numerical value presented in Figure 5.2 corresponds to the minimum energy lattice parameter. The largest value is for the Rh bulk, followed by FeRh and Fe having the smallest lattice parameter. The increase in the bond length value is due to the size of the atomic radii for each atom. Analyzing both dimer and bulk results, it can be appreciated that the bulks have a larger interatomic distance between its atoms.

The results for Fe bulk match with the theoretical value and have a minimum difference of 0.01 Å with the experimental, FeRh bulk match with the theoretical value but present a difference of 0.03 Å. The Rh bulk presents the largest difference compared with the previous works with 0.23 Å.

5.1.3 Nanoclusters

Fe_8Rh_7

The first nanocluster to analyze is the Fe_8Rh_7 formed by a total of 15 atoms: 8 Iron and 7 Rhodium. Figure 5.3 shows the initial topology (left) with an interatomic distance of 2.58 Å for Fe-Rh bond and 2.98 Å between its Fe-Fe and Rh-Rh planes. The structure after the relaxation process (right), whose new lengths will be shown in detail in the following images. All the new bonds and their respective interatomic distances are shown in Figure 5.6.

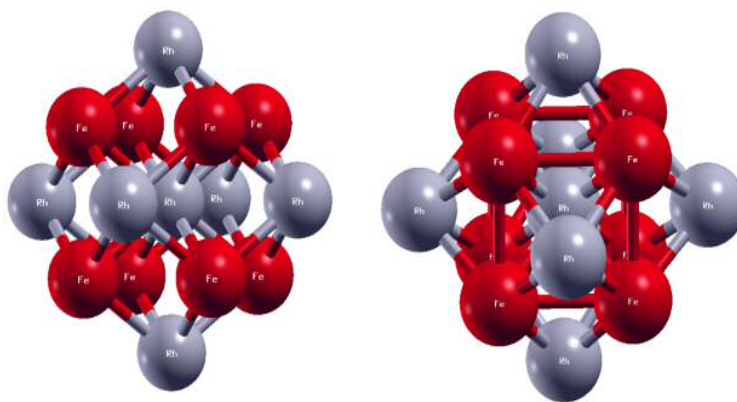


FIGURE 5.3: Illustration of the original structure (left) Fe_8Rh_7 and the change after the relaxation process (right), where dark (light) spheres represent Fe (Rh) atoms.

For the Fe planes Figure 5.4, the relax distance found was 2.66 Å for the 12 Fe bonds, this is a notable change compare it with their original length between the planes was 2.98 Å.

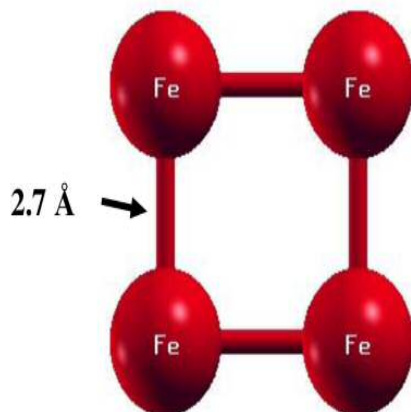


FIGURE 5.4: New Fe bonds after a relaxation process.

For the Rh planes Figure 5.5, the relax distance found was 2.85 Å for the six bonds, exists a decrease in the interatomic length compare with the original distance between its planes was 2.98 Å.

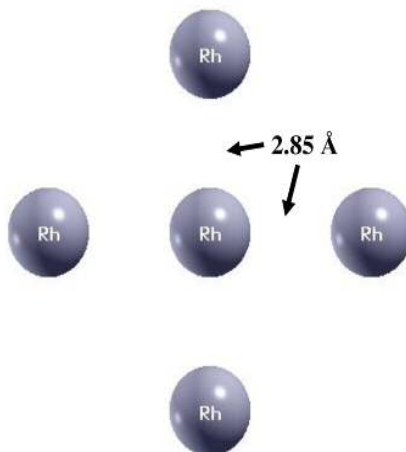


FIGURE 5.5: Change in the interatomic distances between Rh atoms.

These new Fe-Fe and Rh-Rh lengths change the distance of Fe-Rh bonds from 2.58 Å to 32 new bonds, 8 of 2.29 Å, and 24 of 2.42 Å. The nanoclusters size changed due the new bonds from 5.96 to 5.7 Å.

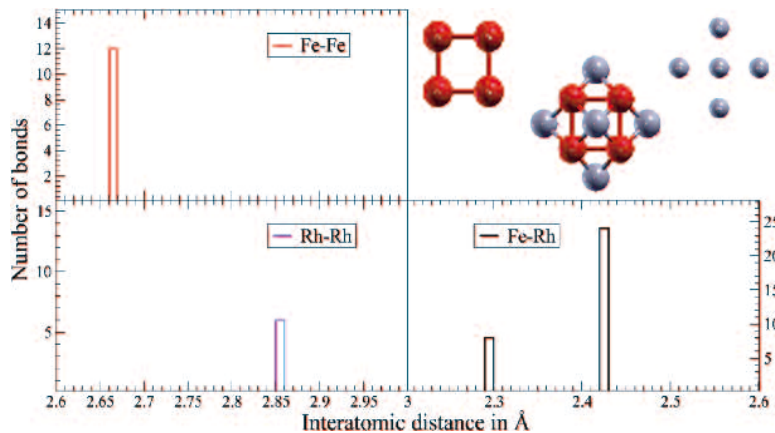


FIGURE 5.6: Number of new bonds Fe-Fe (red), Rh-Rh (violet), and Fe-Rh (black) with their respective interatomic distances.

Figure 5.6 shows the number of bonds versus the interatomic distances of the Fe_8Rh_7 nanocluster. Comparing the new distances present in the nanocluster with the values obtained from the dimers and bulks, conclude the Fe-Fe bond has a closer similarity with Fe bulk lattice parameter with a difference of 0.19 \AA . FeRh 2.42 \AA bond has a close similarity to the bulk value with a difference of 0.56 \AA and FeRh 2.29 \AA with the dimer value with a difference of 0.23 \AA . Rh-Rh bond value is closer to the dimer Rh value with a difference of 0.64 \AA .

$\text{Fe}_{88}\text{Rh}_{81}$

The second nanocluster to analyze is the $\text{Fe}_{88}\text{Rh}_{81}$ formed by a total of 169 atoms 88 Iron and 81 Rhodium, same as for Fe_8Rh_7 , the original distance between Fe-Fe and Rh-Rh planes were 2.98 \AA . For the treatment of this nanocluster, the six Rh atoms in the vertices were removed to have a better similarity with experimental studies. Figure 5.7 shows the original nanocluster (left) and the change in its topology after the relaxation process (right).

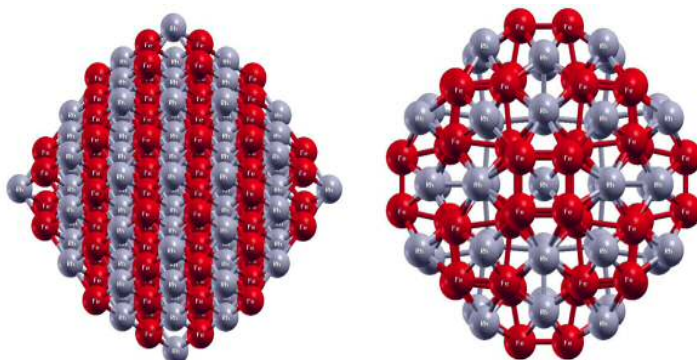


FIGURE 5.7: Illustration of the original structure of $\text{Fe}_{88}\text{Rh}_{81}$ and its respectively structure after relaxation. Dark (light) spheres represents Fe (Rh) atoms.

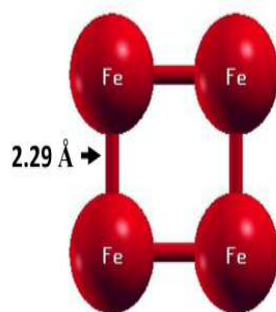


FIGURE 5.8: First Fe plane (4 atoms) after the relaxation process showing the numerical value of the new interatomic distances.

The first Fe plane formed by four atoms Figure 5.8, they change its interatomic distance from 2.98 to 2.29 Å after the relaxation.

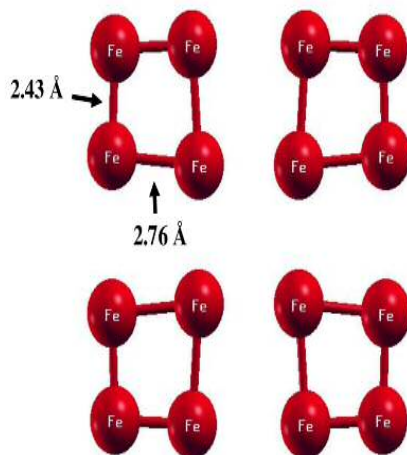


FIGURE 5.9: Second Fe plane (16 atoms) after the relaxation process showing the numerical value for the new interatomic distances.

The second Fe plane constituted by 16 atoms Figure 5.9, which changes its form from a square to four trapezoids, with the side lengths of 2.43 and 2.75 Å.

The third Fe plane is formed by 24 atoms Figure 5.10, the four central atoms form a square with sides of 2.72 Å, the distance of the external bonds is 2.29, 2.58, and 2.76 Å.

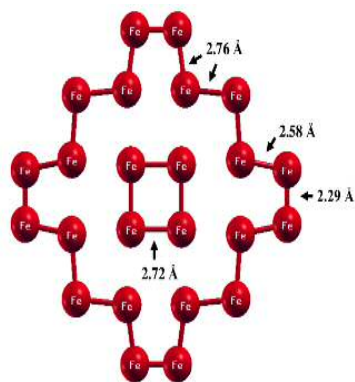


FIGURE 5.10: Third Fe plane (24 atoms) after the relaxation process showing the numerical value of the new interatomic distances.

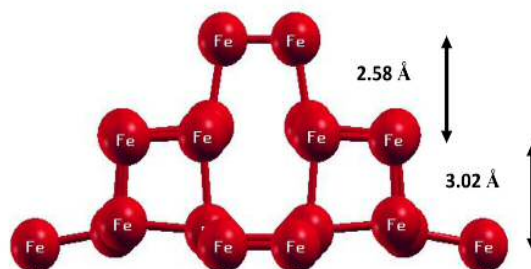


FIGURE 5.11: Illustration of the average distance value of Fe planes.

The initial distance between Fe planes changes, from 2.98 to 2.58 and 3.02 Å, being these distances the average value between the planes.

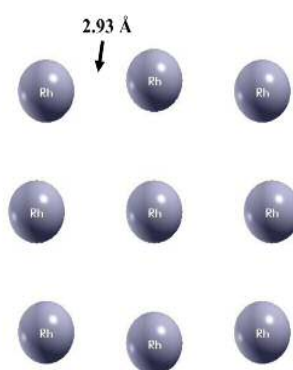


FIGURE 5.12: First Rh plane (9 atoms) after the relaxation process showing the numerical value of the new interatomic distances.

Nine atoms constitute the first Rh plan Figure 5.12, its interatomic distance change from 2.98 to 2.93 Å.

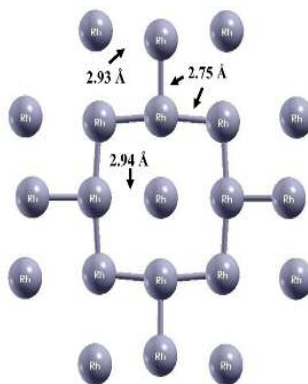


FIGURE 5.13: Second Rh plane (21 atoms) after the relaxation process showing the numerical value of the new interatomic distances.

The second Rh plane is formed by 21 atoms, Figure 2, which presents a decrease in the interatomic distances from 2.98 to 2.75, 2.93, 2.94 Å.

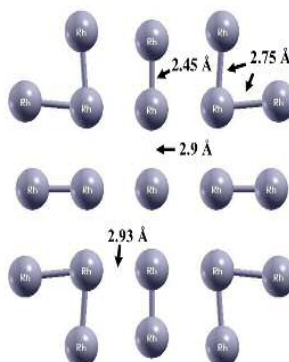


FIGURE 5.14: Third Rh (middle) plane (21 atoms) after the relaxation process showing the numerical value of the new interatomic distances and bonds.

The third Rh plane is constituted by 21 atoms, Figure 5.14, after the relaxation, there is a decrease in the interatomic distances from 2.98 to 2.45, 2.75, 2.9, and 2.93 Å.

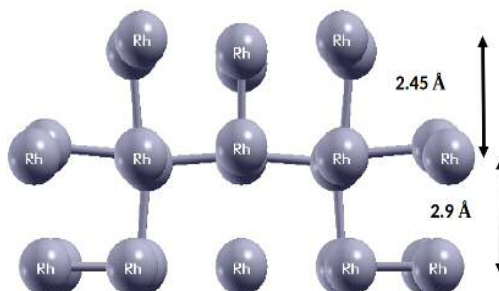


FIGURE 5.15: Illustration of the average distance value of Rh planes

Figure 5.15 shows the average value between the Rh planes after the relaxation. The initial distance between Rh planes changes, from 2.98 to 2.45 and 2.90 Å, being these distances the average value between the planes.

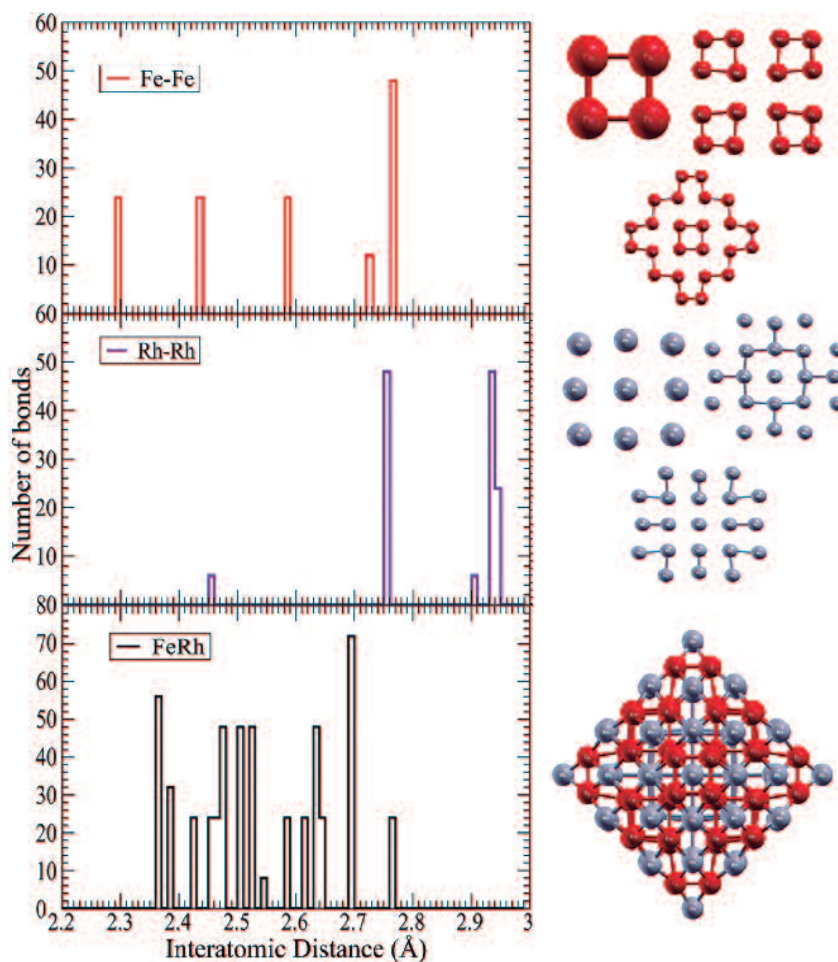


FIGURE 5.16: Number of new bonds Fe-Fe (red), Rh-Rh (violet), and Fe-Rh (black) with their respective interatomic distances.

Figure 5.16 shows the number of bonds versus the interatomic distances of $\text{Fe}_{88}\text{Rh}_{81}$ nanocluster.

Analyzing the distances found in the images for Fe and Rh planes, it can be concluded the largest values correspond to the inner nanocluster atoms and the smallest to the atoms on the surface. Comparing these new distances with the values obtained from the dimers and bulks, they present some similarities, the largest values with the bulks, and the smallest with the dimers.

5.2 Magnetic Properties

5.2.1 Dimers

Dimers have their energy well located Figure 5.17, this is the reason why its DOS has the form of “peaks” and their magnetic moment can be calculated directly, by making the difference between the states with spin-up and spin-down.

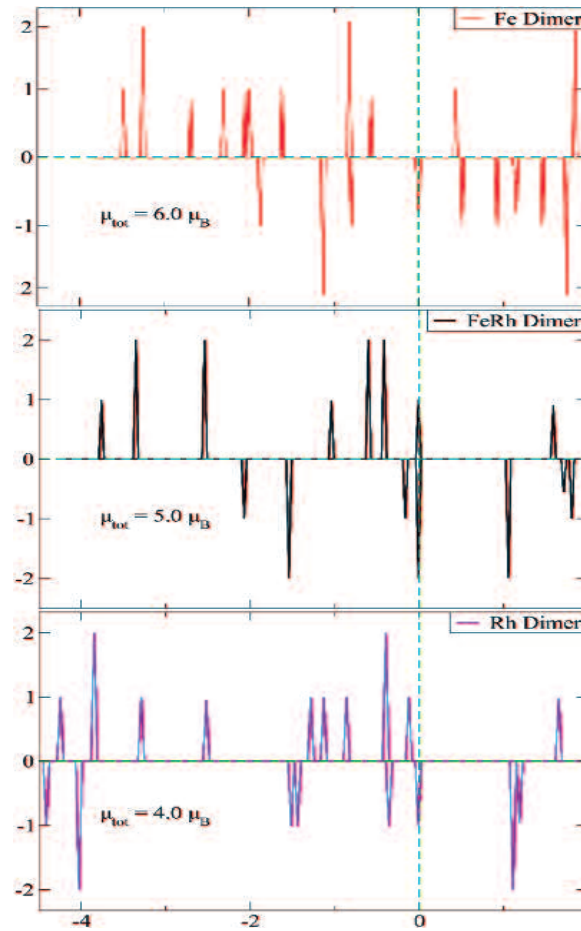


FIGURE 5.17: Illustration of the differences between DOS spin-up and spin-down for Fe_2 , FeRh, and Rh_2 dimers. Positive (negative) values correspond to majority (minority) spin.

Making the difference between DOS in each system, the total magnetic moment found is $6 \mu_B$ for Fe, $5 \mu_B$ for FeRh, and $4 \mu_B$ for Rh. The Fe_2 dimer has the biggest magnetic moment, followed by FeRh, and Rh_2 having the smallest value. These results are compared with previous studies in Table 5.3.

Magnetic Moment (μ_B)			
Dimer	Fe ₂	FeRh	Rh ₂
This Work	6.0	5.0	4.0
Theoretical			
Ref. [38]	5.64	4.67	3.66
Experiment			
Ref. [49]	6.0	5.0	4.0

TABLE 5.3: Total magnetic moment found for Fe₂, Rh₂, and FeRh dimers compared with theoretical and experimental results.

The magnetic moment of this work are close to the corresponding average moments from [38], and match with the reported results from [49].

5.2.2 Bulks

The bulks are systems with more atoms than dimers, this is the reason why their DOS does not have the form of “peaks”, and now it is an actual density Figure 5.18.

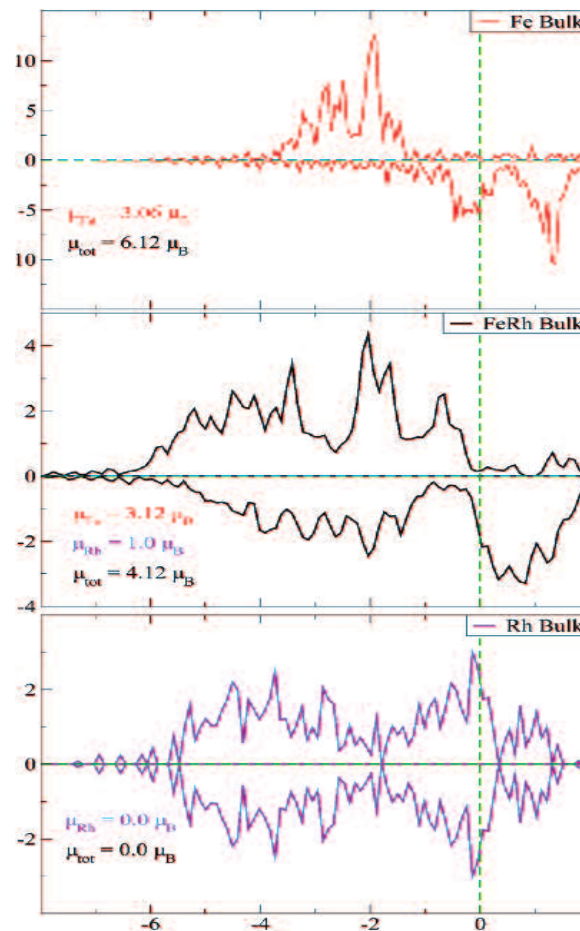


FIGURE 5.18: Illustration of the differences between DOS spin-up and spin-down for Fe, FeRh, and Rh bulks. Positive (negative) values correspond to majority (minority) spin.

Fe and FeRh bulks both have an ferromagnetic (FM) body-centered cubic (BCC) structure and their DOS matches comparing with previous studies. The Rh bulk has an face-centered cubic (FCC) structure, and its DOS corresponds to an antiferromagnetic (AFM) phase, which means its total magnetic moment is zero [50, 51].

Analyzing the magnetic moments from Figure 5.18, the Fe has a total magnetic moment of 6.12, and a moment of $6.12 \mu_B$ per atom, the FeRh has a total magnetic moment of $4.12 \mu_B$ and $3.12 \mu_B$ for the Fe atom and $1.0 \mu_B$ for the Rh atom, and the Rh bulk has a total magnetic moment due to its structure is FCC has AFM phase. These results are compared with previous studies in Table 5.4.

Magnetic moment (μ_B)			
Bulk	Fe	FeRh	Rh
This Work	3.06	$\mu_{Fe}=3.12; \mu_{Rh}=1.0$	0.0
Theoretical			
Ref. [42]	3.0		
Ref. [43]		$\mu_{Fe}=3.11; \mu_{Rh}=1.7$	
Ref. [44]			0.0
Experiment			
Ref. [45]	3.01		
Ref. [46]		$\mu_{Fe}=3.2; \mu_{Rh}=0.9$	
Ref. [47]			0.0

TABLE 5.4: Magnetic moment results for Fe, Rh, and FeRh bulks compared with theoretical and experimental results.

The value obtained in this work for Fe bulk is the largest compare it with the theoretical and experimental results, the Fe atoms the value found is similar to the theoretical but for the Rh atoms have close value with the experiment result for FeRh bulk, and the magnetic moment for Rh bulks have the same value.

5.2.3 Nanoclusters

In this subsection 5.2.3, the density of states and magnetic moment of Fe_8Rh_7 and $\text{Fe}_{88}\text{Rh}_{81}$ are presented and compared with the FeRh bulk results.

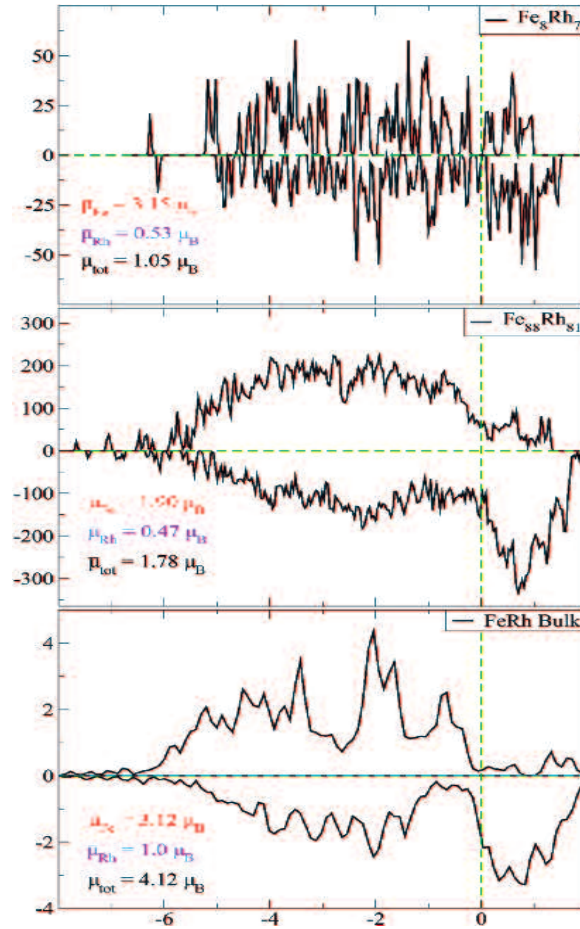


FIGURE 5.19: Illustration of the differences between DOS spin-up and spin-down. Positive (negative) values correspond to majority (minority) spin for Fe_8Rh_7 , $\text{Fe}_{88}\text{Rh}_{81}$ nanoclusters and FeRh bulk

Comparing the DOS for both nanoclusters, it can appreciate the $\text{Fe}_{88}\text{Rh}_{81}$ has a larger density than Fe_8Rh_7 , this is due to the number of atoms in the system, Fe_8Rh_7 is similar to the dimers DOS, and $\text{Fe}_{88}\text{Rh}_{81}$ is analogous to the FeRh bulk DOS form but presents a higher density. The bigger total magnetic moment value is for the $\text{Fe}_{88}\text{Rh}_{81}$ due to the difference between atoms of each system. The largest average magnetic moment value per atom corresponds to the Fe_8Rh_7 with $3.15 \mu_B$ for Fe, $0.53 \mu_B$ for Rh, and the $\text{Fe}_{88}\text{Rh}_{81}$ has $1.90 \mu_B$ for Fe and $0.47 \mu_B$ for Rh. The total average magnetic moment found for Fe_8Rh_7 was $1.05 \mu_B$, and for $\text{Fe}_{88}\text{Rh}_{81}$ was $1.78 \mu_B$.

Chapter 6

Conclusions

After analyzing and discussing the results of the FeRh nanocluster simulations, the following conclusions were reached.

- After the relaxation, the interatomic distances have a notable change where the inner atoms tend to keep interatomic distances alike to the bulk values, and the surface atoms tend to regroup with their nearest neighbors having bond lengths analogous to the dimers.
- The Fe_8Rh_7 DOS has a similar structure with the dimers due to its number of atoms, and $\text{Fe}_{88}\text{Rh}_{81}$ DOS structure tends to the bulk form but presents a higher density, and its geometry is similar to AFM phase.
- Analyzing the magnetic moment results in relation to the nanocluster size it proves the larger the magnetic moment decreases when the system size increases. The reason for this relation is: the particles are so small that a sizeable fraction of the atoms reside at the nanocluster surface. These external atoms carry a larger magnetic moment than the inner ones. The total moment is the sum of all, and the average moment per atom is the sum divided by the number of atoms, as the particle size increased, the average moment decreases because the ratio of the numbers of the surface to inner atoms decreases.

References

- [1] Drexler, Eric. "There's Plenty of Room at the Bottom".
- [2] Efros, A. L., Lockwood, D. J., and Tsybeskov, L. (Eds.). (2013). *Semiconductor Nanocrystals: From Basic Principles to Applications*. Springer Science and Business Media.
- [3] Fallot M. , *Ann. Phys. (N.Y.)* 10, 291 (1938).
- [4] Gruner, M. E., Hoffmann, E., and Entel, P. (2003). Instability of the rhodium magnetic moment as the origin of the metamagnetic phase transition in FeRh. *Physical Review B*, 67(6), 064415.
- [5] Villaseñor-González P., Dorantes-Dávila J., Dreyssé H., and Pastor G. M., *Phys. Rev. B* 55, 15084 (1997).
- [6] Suzuki, I., Koike, T., Itoh, M., Taniyama, T., and Sato, T. (2009). Stability of ferromagnetic state of epitaxially grown ordered FeRh thin films. *Journal of Applied Physics*, 105(7), 07E501.
- [7] Fallot, M. (1938). Les alliages du fer avec les métaux de la famille du platine. In *Annales de Physique* (Vol. 11, pp. 291-332).
- [8] Kudrnovsk, J., Drchal, V., and Turek, I. (2015). Physical properties of FeRh alloys: The antiferromagnetic to ferromagnetic transition. *Physical Review B*, 91(1), 014435.
- [9] Sandratskii, L. M., and Mavropoulos, P. (2011). Magnetic excitations and femtomagnetism of FeRh: A first-principles study. *Physical Review B*, 83(17), 174408.
- [10] Thiele J.-U. , Maat S. , and Fullerton E. E., *Appl. Phys.Lett.* 82, 2859 (2003).
- [11] Buschow, K. H. J. (2003). *Handbook of magnetic materials* (Vol. 15). Elsevier.
- [12] Chikazumi, S., and Graham, C. D. (2009). *Physics of Ferromagnetism 2e* (No. 94). Oxford University Press on Demand.

-
- [13] Kittel, C. (1946). Theory of the dispersion of magnetic permeability in ferromagnetic materials at microwave frequencies. *Physical Review*, 70(5-6), 281.
- [14] Kittel, C. (1976). *Introduction to solid state physics* (Vol. 8). New York: Wiley.
- [15] Jiles, D. (2015). *Introduction to magnetism and magnetic materials*. CRC press.
- [16] Holstein, B. R. (2013). *Topics in advanced quantum mechanics*. Courier Corporation.
- [17] Parr, R. G., and Yang, W. (1995). *Density-functional theory of the electronic structure of molecules*. *Annual review of physical chemistry*, 46(1), 701-728.
- [18] Sakurai, J. J., and Napolitano, J. (2014). *Modern quantum mechanics* (Vol. 185). Harlow: Pearson.
- [19] Payne, M. C., Teter, M. P., Allan, D. C., Arias, T. A., and Joannopoulos, A. J. (1992). Iterative minimization techniques for ab initio total-energy calculations: molecular dynamics and conjugate gradients. *Reviews of modern physics*, 64(4), 1045.
- [20] Sthr, J., and Siegmann, H. C. (2006). *Magnetism. Solid-State Sciences*. Springer, Berlin, Heidelberg, 5.
- [21] Martin, R. M., and Martin, R. M. (2004). *Electronic structure: basic theory and practical methods*. Cambridge university press.
- [22] Hohenberg, P., and Kohn, W. (1964). Inhomogeneous electron gas. *Physical review*, 136(3B), B864.
- [23] Kohn, W., and Sham, L. J. (1965). Self-consistent equations including exchange and correlation effects. *Physical review*, 140(4A), A1133.
- [24] Engel, E., and Dreizler, R. M. (2013). *Density functional theory* (p. 65). Springer-Verlag Berlin An.
- [25] Giustino, F. (2014). *Materials modelling using density functional theory: properties and predictions*. Oxford University Press.
- [26] Blöchl, P. E. (1994). Projector augmented-wave method. *Physical review B*, 50(24), 17953.
- [27] <https://www.vasp.at/>
- [28] Mohn, P. (2006). *Magnetism in the solid state: an introduction* (Vol. 134). Springer Science and Business Media.

- [29] Cherifi, R. O., Ivanovskaya, V., Phillips, L. C., Zobelli, A., Infante, I. C., Jacquet, E., ... and Mougín, A. (2014). Electric-field control of magnetic order above room temperature. *Nature materials*, 13(4), 345.
- [30] Díaz-Sánchez, L. E., Dorantes-Dávila, J., and Pastor, G. M. (2013). Local and chemical environment dependence of the magnetic properties of CoRh core-shell nanoparticles. *Physical Review B*, 88(13), 134423.
- [31] Dupuis, V., Blanc, N., Daz-Snchez, L. E., Hillion, A., Tamion, A., Tournus, F., and Pastor, G. M. (2013). Specific local relaxation and magnetism in mass-selected CoPt nanoparticles. *The European Physical Journal B*, 86(3), 83. 28
- [32] Jia Z. , Seetala N. , and Misra R. , *Physica (Amsterdam)* 405, 2189 (2010).
- [33] Blanc, N., Díaz-Sánchez, L. E., Ramos, A. Y., Tournus, F., Tolentino, H. C. N., De Santis, M., ... and Boisron, O. (2013). Element-specific quantitative determination of the local atomic order in CoPt alloy nanoparticles: Experiment and theory. *Physical Review B*, 87(15), 155412.
- [34] Bertaut E., Delapalme A., Forrat F., Roult G., de Bergevin F., and Pauthenet R., *Appl J. Phys.* 33, 1123 (1962).
- [35] Cox A. J. , Louderback J. G. , and Bloomfield L. A. , *Phys.Rev. Lett.* 71, 923 (1993); A. J. Cox, J. G. Louderback, S. E. Apsel, and L. A. Bloomfield, *Phys. Rev. B* 49, 12295 (1994).
- [36] Dorantes-Dávila J. , Dreyssé H. , and Pastor G. M. , *Phys. Rev. B* 46, 10432 (1992).
- [37] Harutyunyan A. R. , Awasthi N. , Jiang, W. Setyawan A. , Mora E. , Tokune T. , Bolton K. , and Curtarolo S. , *Phys.Rev.Lett.* 100, 195502 (2008).
- [38] Mokka, J. H., and Pastor, G. M. (2012). Interplay between chemical and magnetic order in FeRh clusters. *The Journal of Physical Chemistry C*, 116(32), 17228-17238.
- [39] Rollmann, G., Herper, H. C., and Entel, P. (2006). Electron correlation effects in the Fe dimer. *The Journal of Physical Chemistry A*, 110(37), 10799-10804.
- [40] Moulton, R. D., Chandler, D. J., Arif, A. M., Jones, R. A., and Bard, A. J. (1988). Synthesis and electrochemistry of $(\text{CO})_2(\text{PMe}_3)_2\text{Fe}(\mu\text{-}2\text{-tert-Bu}_2\text{P})_2(\mu\text{-}2\text{-CO})\text{Rh}(\text{PMe}_3)_2$ (Fe-Rh)(L= CO, PMe_3). Digital simulation of modified ECE mechanism. X-ray crystal structures of $(\text{CO})_2(\text{PMe}_3)_2\text{Fe}(\mu\text{-}2\text{-tert-Bu}_2\text{P})_2(\mu\text{-}2\text{-CO})\text{Rh}(\text{PMe}_3)_2$ and $[\text{Me}_3\text{PO} \cdot \text{Na}(15\text{-crown-}5)] + [(\text{CO})_3\text{Fe}(\mu\text{-}2\text{-tert-Bu}_2\text{P})\text{Rh}(\text{PMe}_3)(\text{CO})]^-$. *Journal of the American Chemical Society*, 110(17), 5714-5725.

-
- [41] Beltrán, M. R., Zamudio, F. B., Chauhan, V., Sen, P., Wang, H., Ko, Y. J., and Bowen, K. (2013). Ab initio and anion photoelectron studies of Rh n ($n= 1-9$) clusters. *The European Physical Journal D*, 67(3), 63.
- [42] Davey, Wheeler (1925). Precision Measurements of the Lattice Constants of Twelve Common Metals. *Physical Review*. 25 (6): 753-761.
- [43] Aschauer, U., Braddell, R., Brechbhl, S. A., Derlet, P. M., and Spaldin, N. A. (2016). Strain-induced structural instability in FeRh. *Physical Review B*, 94(1), 014109.
- [44] Xin, C., Jian-Tao, W., Xi-Xia, L., and Guo-Zhong, Z. (2010). Mechanical and Magnetic Properties of Rh and RhH: First-Principles Calculations. *Chinese Physics Letters*, 27(2), 027101.
- [45] Jephcoat, A. P., Mao, H. K., and Bell, P. M. (1986). Static compression of iron to 78 GPa with rare gas solids as pressure-transmitting media. *Journal of Geophysical Research: Solid Earth*, 91(B5), 4677-4684.
- [46] G. Shirane, R. Nathans, and C. W. Chen, *Phys Rev* 134,A1547 (1964).
- [47] Ahmed, S., Zafar, M., Shakil, M., and Choudhary, M. A. (2015). Ab initio study of structural, electronic, and thermal properties of Ir $_{1-x}$ Rh $_x$ alloys. arXiv preprint arXiv:1506.03966.
- [48] Harrison, W. A. (2012). *Electronic structure and the properties of solids: the physics of the chemical bond*. Courier Corporation.
- [49] Bader, R. F. W. *Atoms in Molecules, A Quantum Theory*; Oxford University Press: Oxford, 1990.
- [50] Muldrew, L., and DeBergevin, F. (1961). Antiferromagnetic-Ferromagnetic Transformation in FeRh. *The Journal of Chemical Physics*, 35(5), 1904-1905.
- [51] Polatoglou, H. M., Methfessel, M., and Scheffler, M. (1993). Vacancy-formation energies at the (111) surface and in bulk Al, Cu, Ag, and Rh. *Physical Review B*, 48(3), 1877.